Microscopic investigation of the superconducting properties of the strongly coupled superconductor IrGe via μSR

Arushi,[1] Kapil Motla,[1] P. K. Meena,[1] S. Sharma ©,[1] D. Singh,[2] P. K. Biswas,[2] A. D. Hillier ©,[2] and R. P. Singh ©[1,*]

[1]*Department of Physics, Indian Institute of Science Education and Research Bhopal, Bhopal 462066, India*
[2]*ISIS Facility, STFC Rutherford Appleton Laboratory, Harwell Science and Innovation Campus, Oxfordshire OX11 0QX, United Kingdom*

Exploring superconductors which can possess a pairing mechanism other than the BCS predicted s wave have continually attracted considerable interest. Superconductors with low-lying phonons may exhibit unconventional superconductivity as the coupling of electrons with these low-lying phonons can potentially affect the nature of the superconducting ground state, resulting in strongly coupled superconductivity. In this work, by using magnetization, AC transport, specific heat, and muon spin rotation/relaxation (μSR) measurements, we report a detailed investigation on the superconducting ground state of the strongly coupled superconductor, IrGe, that has a transition temperature, T_C, at 4.7 K. Specific heat (SH), and transverse field μSR is best described with an isotropic s-wave model with strong electron-phonon coupling, indicated by the values of both $\Delta(0)/k_B T_C = 2.3, 2.1$ (SH,μSR), and $\Delta C_{el}/\gamma_n T_C = 2.7$. Zero-field μSR measurements confirm the presence of time-reversal symmetry in the superconducting state of IrGe.

I. INTRODUCTION

Understanding the pairing mechanism of unconventional superconductors is an active area of ongoing research in the field of superconductivity. In contrast to conventional superconductors, where spin-singlet superconductivity is explained by weak electron-phonon coupling, in unconventional superconductors, the proposed pairing mechanisms strongly depend on the observed exotic features together with other symmetries present in them and cannot be generalized to all [1–9]. Superconductors with low-lying phonons emerged as a class of unconventional superconductors with a very strongly coupled superconductivity [10–17]. In these superconductors, the low-lying phonons originated from the rattling modes are proposed and it is also suggested that electron-rattler phonon mode coupling mediates the Cooper pairing, resulting in the extremely strong-coupled superconductivity. These excitations may behave differently from the usual phonons, which give rise to conventional BCS superconductivity and may have an impact on the order parameter symmetry. Only a few superconductors with low-lying phonons resulting in a strong coupling have been studied via microscopic and macroscopic measurements. It provides the presence of an isotropic energy gap in $RbOs_2O_6$ [18], anisotropic or multigap with small energy in KOs_2O_6 [19], and multiband superconductivity in $SrPt_3P$ [20] and Nb_5Ir_3O [21]. The existence of exotic superconducting gap structures and strong electron-phonon coupling in these compounds may hint towards the role of low-lying phonons and requires a schematic study of more compounds that fall into this category to completely understand the role of low-lying phonons on the nature of superconducting ground state properties.

The transition metal germanide, IrGe, is also known to exhibit strongly coupled superconductivity with a high value of specific heat jump ($C_{el}/\gamma_n T_C = 3.04$) and superconducting gap [$\Delta(0)/k_B T_C = 2.57$] [22]. The Debye temperature from the specific heat measurements gives $\theta_D = 160$ K, which is almost half of the similar molar mass compound, PtGe. Phonon density of state calculations suggest the presence of low-lying phonons in IrGe [23]. The obtained Einstein temperature from specific heat measurement accounts for the energy of low-lying phonons, which falls in the temperature range calculated for the rattling modes in superconducting pyrochlore osmates [22] where these modes are considered as the origin of low-lying phonons [19]. Moreover, the density of states at the Fermi level is mainly dominated by the Ir $5d$ states [23] which can induce strong spin-orbit coupling (SOC) effects and also the emergence of $5d$ superconductivity. Therefore, the correlation between unconventional superconductivity and strong SOC, and to examine the influence of low-lying excitations on the nature of superconducting ground state warrants a thorough investigation on IrGe through a microscopic tool such as muon spin rotation/relaxation (μSR). This study will also serve as a reference for the strongly coupled low-lying phonon mediated superconductors.

In this paper, we report the superconducting ground state properties of IrGe through different techniques such as AC transport, magnetization, specific heat, and μSR. Bulk superconductivity was confirmed from all the mentioned measurements at $T_C = 4.74(3)$ K. Transverse field μSR measurements together with specific heat reveal a nodeless s-wave superconducting gap with strong electron-phonon coupling. Zero-field μSR measurements confirm the presence of time-reversal symmetry in IrGe.

*rpsingh@iiserb.ac.in

II. EXPERIMENTAL DETAILS

The polycrystalline sample of IrGe was prepared by the solid-state reaction method described in the Ref. [22]. A powder x-ray diffraction (XRD) experiment was conducted using a PANalytical X'Pert Pro diffractometer equipped with Cu $K\alpha$ radiation ($\lambda = 1.5406$ Å). A Quantum Design superconducting quantum interference device (SQUID) was used to collect magnetization data in the temperature range of 1.8–7.0 K with various applied fields. Specific heat measurements and AC transport without and with fields were performed on a Quantum Design physical property measurement system (PPMS). Specific heat measurements employed a two-tau relaxation method whereas for AC transport, a four probe method was used. The μSR measurements were conducted at the ISIS Neutron and Muon Facility, STFC Rutherford Appleton Laboratory, United Kingdom using the MUSR spectrometers in both the longitudinal and transverse directions [24]. The powdered sample of IrGe was mounted on a silver (99.995%) holder using GE varnish and inserted in the sample chamber of a He-3 sorption cryostat. One hundred percent spin-polarized muons were implanted into the sample which decays into positrons and neutrinos after a mean lifetime of 2.2 μs. The decayed positrons are emitted preferentially in the direction related to the orientation of the muon spin vector and were collected by either forward (F) or backward (B) detectors in longitudinal configuration. The time-dependent asymmetry $G_z(t)$ is the measured quantity and is calculated as $[N_F(t) - \alpha N_B(t)]/[N_F(t) + \alpha N_B(t)]$, where $N_F(t)$ and $N_B(t)$ are the number of positron counts in the forward and backward detector, respectively. α is an instrumental calibration factor which represents the efficiency for relative counting between F and B detectors. Thus, the time evolution of muon polarization [calculated from $G_z(t)$] allows one to determine the local magnetic environment experienced by the muon ensemble. Zero-field (ZF) measurements were carried out with detectors placed in longitudinal configuration. To achieve true zero fields, stray magnetic fields (originated from Earth and neighboring instruments) were canceled within 1 μT limit by a fluxgate magnetometer and an active compensation system controlling three pairs of correction coils. In transverse field (TF) measurements, a field perpendicular to the initial muon spin polarization direction was applied. TF measurements for IrGe were performed in the vortex state by applying a field of 50 mT in field cooled condition.

III. RESULTS AND DISCUSSION

A. Sample characterization

Rietveld refinement shown in Fig. 1 confirms that material crystallizes in orthorhombic structure with space group *Pnma* [22]. The lattice parameters and atomic positions obtained from the refinement are given in Table I.

B. Normal and superconducting state properties

The main panel of Fig. 2 displays the temperature dependence of resistivity, $\rho(T)$, above the superconducting state and in zero applied field. The inset in the top left corner shows the enlarged view of $\rho(T)$ in the low-temperature regime where
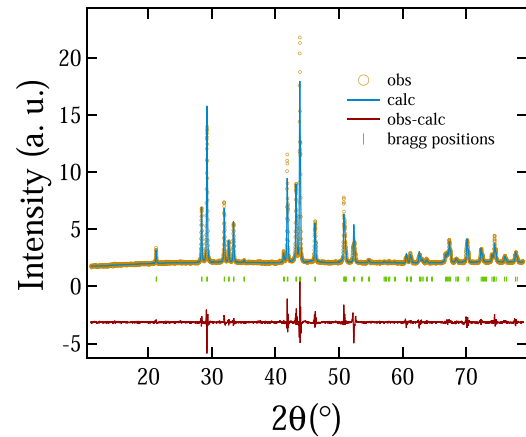

FIG. 1. Room temperature powder XRD pattern of IrGe is shown by yellow circles whereas the blue line represents the Rietveld refinement. Bragg positions are shown by green vertical bars and the red solid line displays the difference between the calculated and observed patterns.

it exhibits a drop in resistivity value at $T_{C,\text{onset}} = 4.7(1)$ K and the zero resistance state is achieved at $T_{C,0} = 4.6(1)$ K with a width of superconducting transition, $\Delta T = 0.1$ K. The normal state $\rho(T)$ shows an almost linear T dependence down to low temperatures similar to a strongly coupled superconductor $SrPt_3P$ [15] where such behavior is attributed to the presence of low-lying excitations. At high temperatures, the resistivity curve seems to saturate, which implies that the mean free path of electrons reaches the order of interatomic spacing. A similar response is observed for other strongly coupled A15 superconductors [25] and $SrPt_3P$ [15] where the saturation of resistivity is interpreted as the strong coupling between the charge carriers and phonons. Hall measurement was also performed to calculate the carrier concentration and the type of charge carriers. The inset in the bottom right shows the field dependence of Hall resistivity (ρ_{xy}) measured at $T = 100$ K. $\rho_{xy}(H)$ is well described by a straight line fit and provides a slope which is the Hall coefficient $R_H = 4.9(1) \times 10^{-8}$ Ω cm/T. The positive sign indicates the hole carrier concentration, and the relation $R_H = 1/ne$ yields $n = 1.27(2) \times 10^{-28}$ m^{-3}.

Magnetic susceptibility of IrGe in an applied field of 1 mT via two different modes, (i) zero-field cooled warming (ZFCW) and (ii) field cooled cooling (FCC), is shown in Fig. 3(a). It exhibits a clear diamagnetic signal below a

TABLE I. Parameters obtained from Rietveld refinement of IrGe.

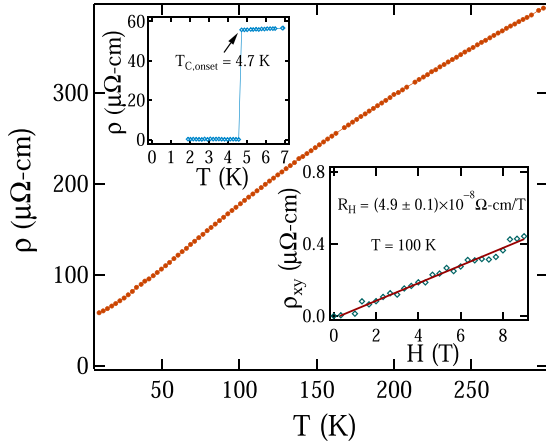|	Structure		Orthorhombic	
	Space group		*Pnma*	
	Lattice parameters			
	a (Å)		5.6000(1)	
	b (Å)		3.4935(1)	
	c (Å)		6.2865(1)	
Atom	Wyckoff position	x	y	z
Ir	4c	0.00141	0.25000	0.20324
Ge	4c	0.18524	0.25000	0.58013

FIG. 2. Temperature dependence of resistivity in the temperature range $10 \text{ K} \leqslant T \leqslant 300 \text{ K}$. The inset in the top left corner shows the resistivity drop at $T_{C,\text{onset}} = 4.7(1)$ K. The bottom right inset represents the field variation of Hall resistivity up to $+9T$ at $T = 100$ K.

transition temperature, $T_C = 4.74(3)$ K and confirms the bulk superconductivity. The difference in the magnitude of the FCC diamagnetic signal than in the ZFCW can be accounted for due to the strong flux pinning present in the material. To calculate the lower critical field, $H_{C1}(0)$, low-field magnetization curves were obtained at different temperatures, from 1.9 to 4.3 K. H_{C1} is defined as the point deviating from the initial slope of the linear or Meissner line for individual temperature curves. The corresponding data sets are shown in Fig. 3(b) and fitted with the Ginzburg-Landau relation given below and yield $H_{C1}(0) = 13.3(2)$ mT:

$$H_{C1}(T) = H_{C1}(0)\left[1 - \left(\frac{T}{T_C}\right)^2\right]. \qquad (1)$$

The upper critical field $H_{C2}(0)$ is obtained from a range of measurements: magnetization, resistivity, and specific heat (see Fig. 4, right inset) at different applied fields. In magnetization, the onset of superconductivity is taken as the criteria for T_C, whereas in specific heat and resistivity, the midpoint is considered as the transition temperature. Figure 3(c) represents $H_{C2}(T)$ from all measurements, and it follows a linear behavior near $T = T_C$ that can be fitted well with the phenomenological Ginzburg-Landau expression below where $t = T/T_C$. The fit provides $H_{C2}(0) = 1.13(2)$ T.

$$H_{C2}(T) = H_{C2}(0)\frac{[1 - t^2]}{[1 + t^2]}. \qquad (2)$$

There are two main mechanisms that can destroy superconductivity: (a) orbital limiting effect and (b) Pauli paramagnetic limit. When the kinetic energy of Cooper pairs exceeds the condensation energy, the orbital effect comes into play, whereas in the case of the Pauli limiting effect, the spin of one of the electrons in a Cooper pair is oriented in the direction of the applied field, which in turn destroys superconductivity. The orbital limit of an upper critical field, $H_{C2}^{\text{orb}}(0)$ for a type II dirty limit superconductor (see Sec. III D) is given by [26,27]

$$H_{C2}^{\text{orb}}(0) = -\alpha T_C \left.\frac{dH_{C2}(T)}{dT}\right|_{T=T_C}, \qquad (3)$$

where $\alpha = 0.693$ for dirty limit superconductors, $T_C = 4.74(3)$ K, and the slope at $T = T_C$ is given by 0.21(3) T and yields $H_{C2}^{\text{orb}}(0) = 0.68(2)$ T. The Pauli limiting field is given by [28,29] $H_{C2}^P = 1.86T_C$, and $T_C = 4.74$ K. It provides $H_{C2}^P = 8.74(2)$ T. The Maki parameter describes the relative importance of both the orbital and paramagnetic effects in suppressing superconductivity and is given by [30] $\alpha_M = \sqrt{2}H_{C2}^{\text{orb}}(0)/H_{C2}^p(0) = 0.11(2)$. The obtained value of α_M is significantly less than unity, suggesting that the influence of the Pauli limiting effect is small. The two fundamental length scales of any superconductor are the coherence length $\xi_{GL}(0)$ and penetration depth $\lambda_{GL}(0)$. These are calculated from $H_{C1}(0)$ and $H_{C2}(0)$. $\xi_{GL}(0)$ is 170(1) Å using the formula [31] $H_{C2}(0) = \frac{\Phi_0}{2\pi\xi_{GL}^2}$ where $\Phi_0(= 2.07 \times 10^{-15}$ T m$^2)$ is the magnetic flux quantum and $H_{C2}(0) = 1.13(2)$ T. The London penetration depth [$\lambda_{GL}(0)$] is calculated using the expression [32]

$$H_{C1}(0) = \frac{\Phi_0}{4\pi\lambda_{GL}^2(0)}\left(\ln\frac{\lambda_{GL}(0)}{\xi_{GL}(0)} + 0.12\right), \qquad (4)$$

which takes into account both $\xi_{GL}(0) = 170(1)$ Å and $H_{C1}(0) = 13.3(2)$ mT, and provides $\lambda_{GL}(0) = 1750(11)$ Å. The Ginzburg-Landau parameter is given by $\kappa_{GL} = \frac{\lambda_{GL}(0)}{\xi_{GL}(0)} = 10(1) > 1/\sqrt{2}$, which classifies IrGe as a type II superconductor. The thermodynamic critical field $H_C(0)$ was estimated using the relation $H_{C1}(0)H_{C2}(0) = H_C(0)^2\ln\kappa_{GL}$ [32], which yields $H_C(0)$ as 78 mT.

The inset of Fig. 4 presents the temperature dependence of the specific heat at zero applied field. A sharp jump at $T_C = 4.6$ K is evidence of bulk superconductivity. The normal state data was fitted with the formula $C = \gamma_n T + \beta_3 T^3$ where γ_n is the Sommerfeld constant of the normal state, and β_3 represents the specific heat coefficient of the lattice part. The fit provides $\gamma_n = 3.1(2)$ mJ mol^{-1} K^{-2} and $\beta_3 = 0.94(1)$ mJ mol^{-1} K^{-4}. The Debye temperature can be written as $\theta_D = (12\pi^4 RN/5\beta_3)^{1/3}$ [33] where $R = 8.314$ J mol^{-1} K^{-2} is a gas constant, and $N = 2$ is the number of atoms in the formula unit. Using the relation, we obtained $\theta_D = 160(1)$ K. The McMillan [34] model is used to evaluate the strength of electron-phonon coupling, $\lambda_{e\text{-}ph}$, which is related to θ_D and T_C as follows:

$$\lambda_{e\text{-}ph} = \frac{1.04 + \mu^*\ln(\theta_D/1.45T_C)}{(1 - 0.62\mu^*)\ln(\theta_D/1.45T_C) - 1.04}. \qquad (5)$$

Here μ^* represents the screened Coulomb potential and is taken to be 0.13. The calculated value of $\lambda_{e\text{-}ph} = 0.78(2)$ indicates the strong electron-phonon coupling in the superconducting state of IrGe. To determine the electronic contribution of the specific heat, we have subtracted the phononic part ($\beta_3 T^3$) from the total specific heat (C). Low-temperature electronic specific heat data can tell us about the nature of the superconducting gap structure, and in this regard, the normalized electronic specific heat was fitted, and yields an excellent fit, with just a single isotropic s-wave gap expression which is related to the normalized entropy by

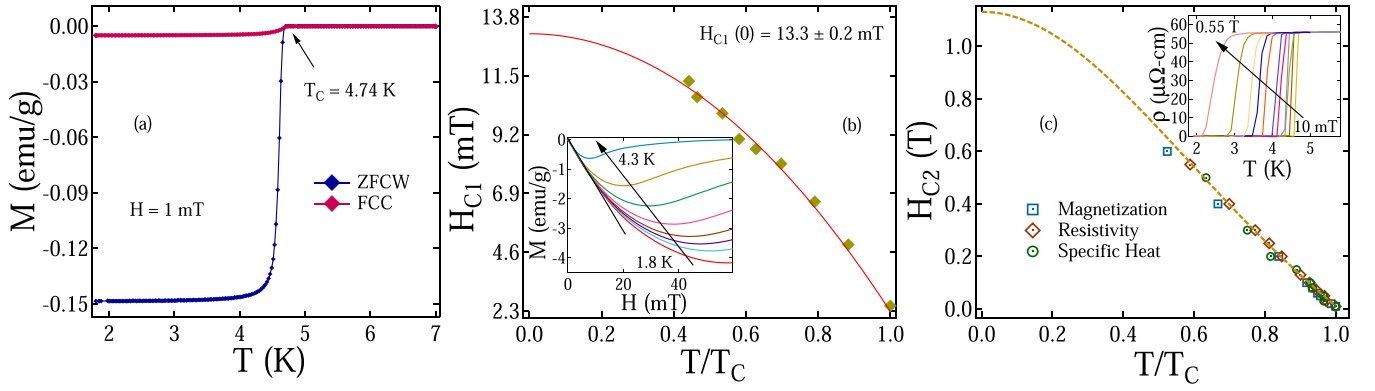$$\frac{C_{el}}{\gamma_n T_C} = t\frac{d(S/\gamma_n T_C)}{dt}, \qquad (6)$$

FIG. 3. (a) The magnetic moment with respect to temperature measured at 1 mT. (b) The lower critical field vs temperature where the inset shows the low-field magnetization curves at various temperatures. (c) The temperature dependence of the upper critical field from various measurements where the inset shows the field and temperature variations of ρ.

where the BCS expression for the normalized entropy is provided below:

$$\frac{S}{\gamma_n T_C} = -\frac{6}{\pi^2}\left(\frac{\Delta(0)}{k_B T_C}\right)\int_0^\infty [f\ln(f) + (1-f)\ln(1-f)]dy,$$

(7)

where $f(\xi) = \{\exp[E(\xi)/k_B T] + 1\}^{-1}$ is the Fermi function, $E(\xi) = \sqrt{\xi^2 + \Delta^2(t)}$, where $E(\xi)$ is the energy of the normal electrons measured relative to Fermi energy, $y = \xi/\Delta(0)$, $t = T/T_C$, and $\Delta(t) = \tanh[1.82\{1.018[(1/t) - 1]\}^{0.51}]$ is the BCS approximation for the temperature dependence of energy gap. The expression provides a good fit to the data shown by a red solid line in Fig. 4 with the gap value $\Delta(0)/k_B T_C = 2.3(1)$. The value of the gap significantly exceeds that of the predicted BCS value, 1.76, and suggests that strongly coupled superconductivity is present in IrGe.
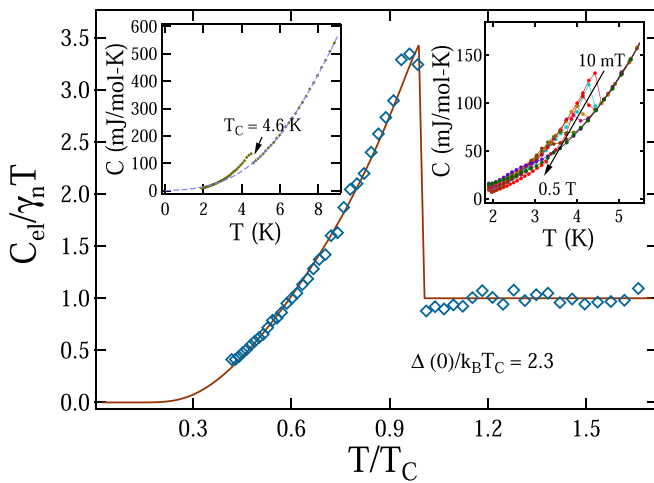
C. Muon spin rotation and relaxation

Zero-field μSR measurements were performed to confirm the presence of possible magnetism and/or breaking of time-reversal symmetry in the superconducting state of IrGe. Figure 5 presents the time evolution of ZF μSR asymmetry spectra collected above and below T_C. For broken TRS, the onset of spontaneous magnetization causes an increase in the relaxation rate in the superconducting state [35]. However, for our case, there is no change in the relaxation rate across T_C within the detection limit of μSR, which confirms the absence of time-reversal symmetry breaking in IrGe. Both the spectra are well described with a static Kubo-Toyabe times exponential decay function plus a flat background term given below [36]:

$$A(t) = A_0\left[\frac{1}{3} + \frac{2}{3}\left(1 - \sigma_{zf}^2 t^2\right)\exp\left(-\frac{1}{2}\sigma_{zf}^2 t^2\right)\right]\exp(-\Lambda t)$$
$$+ A_{bg}.$$

(8)

Here σ_{zf} is the muon spin relaxation arising from the randomly oriented, static local fields associated with nuclear moments at the muon site. Λ is associated with the electronic relaxation rate, probably from the Ir. A_0 and A_{bg} are the initial asymmetry contribution from the sample and back-
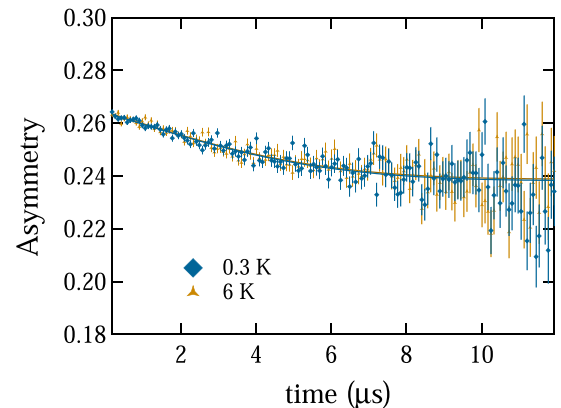

FIG. 4. Temperature dependence of normalized specific heat in zero applied fields where the solid red line is a fit using the isotropic *s*-wave model. Inset (left): Specific heat variation with T which exhibits a sharp jump at $T_C = 4.6$ K. Dotted line is a fit using $C = \gamma_n T + \beta_3 T^3$ to calculate the electronic and phononic contributions. Inset (right): Specific heat with respect to temperature at various applied fields starting from 10 mT to 0.5 T.

FIG. 5. Time-domain ZF-μSR spectra of IrGe in the superconducting (0.3 K) and normal state (6.0 K). The solid lines are fit using Eq. (8).

ground asymmetry which is constant and nondecaying in nature. Solid lines show the fits for both temperatures with $A_0 \sim 0.025$. One of the possible reasons for such a small value of A_0 might be the presence of a very slowly relaxing component in ZF spectra which is not relaxed fully in the measured timescale; therefore, it led to a higher value of A_{bg} in our case. Similar values of A_0 for ZF spectra are also reported for Re$_3$W (centrosymmetric phase) [37] and LaPt$_3$P [38]. σ_{zf} is found to be 0.134 μs^{-1} and the field strength corresponding to the difference in the relaxation rate (Λ) for above and below T_C is 0.04 G, which is outside the detection limit of μSR measurement. This clearly suggests the preserved time-reversal symmetry in the superconducting ground state of IrGe within the detection limit of μSR.

To explore the nature of the superconducting gap in IrGe at a microscopic level, μSR measurements in transverse applied fields were carried out. Experiments were performed in field cooled conditions in which a transverse field of 50 mT was applied in the normal state to ensure a formation of well-ordered flux-line lattices, and data were collected while warming. The typical polarization spectra in 50 mT collected above and below T_C are presented in Fig. 6(a). The enhanced depolarization rate below T_C reflects the inhomogeneous field distribution of the flux-line lattice (FLL) in the mixed state. The reduced depolarization above T_C is due to the randomly oriented static, on the timescale of the muon, nuclear moments. The TF spectra can be modeled by a sum of N sinusoidal oscillating functions, each damped with a Gaussian relaxation envelope plus a flat background term [39,40]

$$A(t) = \sum_{i=1}^{N} A_i \exp\left(-\frac{1}{2}\sigma_i^2 t^2\right) \cos(\gamma_\mu B_i t + \phi) + A_{bg}. \quad (9)$$

A_i, B_i, σ_i, ϕ, and $\gamma_\mu/2\pi = 135.5$ MHz/T are initial asymmetry, first moment for the ith component of the field distribution, Gaussian relaxation rate, initial phase offset, and muon gyromagnetic ratio, respectively. In this case, $N = 2$ oscillating functions were sufficient to fit the data where the relaxation from the second component (σ_2) was fixed to zero. It considers the nodepolarizing muons that missed the sample and hit the sample holder. In Eq. (9), an additional $\exp(-\Lambda t)$ term in multiplication with the $N = 1$ function is not incorporated as the relaxation corresponding to this term is weak compared to the precession signal resulting from the formation of the vortex lattice. Therefore, its absence will not affect the computed results from TF data. The bottom left inset of Fig. 6(b) shows the internal field distribution with respect to the measured temperature range. B_{bg} corresponds to the background field which is temperature independent, whereas $\langle B \rangle$ represents the expulsion of the magnetic field on entering the superconducting state by reducing the strength of the applied field (B_{app}) below T_C and recovers to B_{app} above T_C. To calculate the flux-line lattice state contribution to the relaxation rate (σ_{FLL}), the extra broadening arising from the nuclear moments (σ_N) must be subtracted in quadrature from σ using $\sigma_{FLL} = (\sigma^2 - \sigma_N^2)^{1/2}$. As σ_N is expected to be temperature independent, its contribution can be taken from the normal state σ value shown by a horizontal line in the upper right inset of Fig. 6(b). The value of σ_N is considered to be 0.161 μs^{-1}. Figure 6(b), main panel, shows the temperature
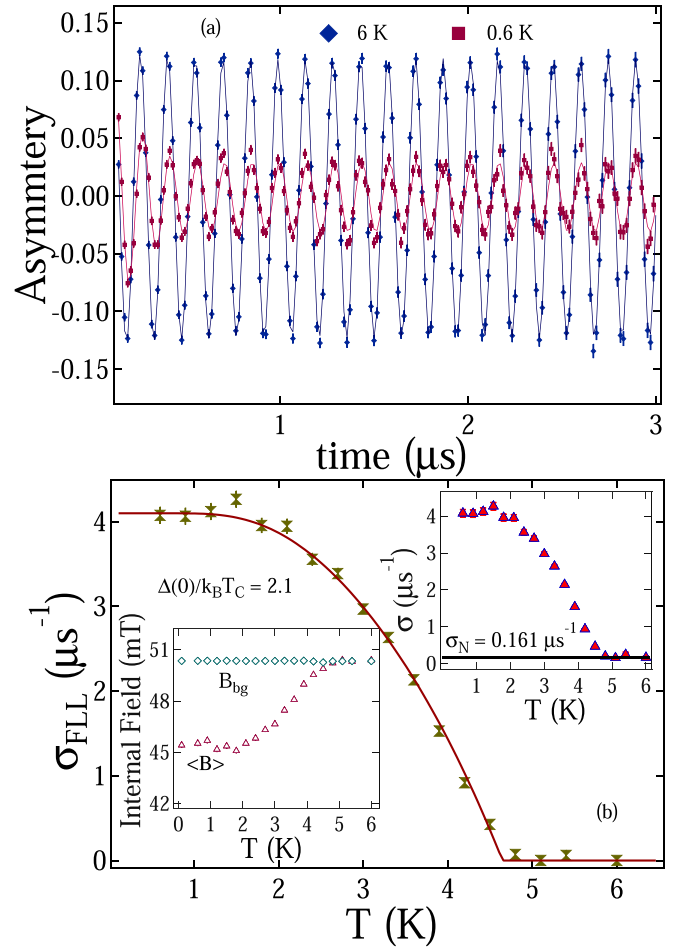

FIG. 6. (a) TF-μSR asymmetry spectra collected above (6.0 K) and below (0.6 K) T_C shows different relaxation rates. (b) Flux-line lattice contribution to the relaxation rate vs temperature as determined from TF-μSR spectra where the solid line is a fit using the s-wave superconducting gap function. Inset: Temperature dependence of internal magnetic field distribution (bottom left) and total depolarization rate (upper right).

dependence of σ_{FLL} and is related to penetration depth via $\lambda^{-2} \propto \sigma_{FLL}$. Considering London local electrodynamics, the temperature dependence of penetration depth for the s-wave superconductor in dirty limit (see Sec. III D) was modeled using

$$\frac{\sigma_{FLL}(T)}{\sigma_{FLL}(0)} = \frac{\lambda^{-2}(T)}{\lambda^{-2}(0)} = \frac{\Delta(T)}{\Delta(0)}\tanh\left[\frac{\Delta(T)}{2k_B T}\right], \quad (10)$$

where $\Delta(T) = \Delta_0\tanh(1.82\{1.018[(T_C/T) - 1]\}^{0.51})$ is the BCS approximation for the temperature dependence of the energy gap. The function provides the best fit to the data which is represented by the solid red line, and yields the superconducting gap value, $\Delta_0/k_B T_C = 2.1$ (1). The obtained value is in agreement with the specific heat results and is significantly higher than the predicted BCS value. It indicates a strong-coupling nature of the superconducting pairs in IrGe. The presence of strong electron-phonon coupling can be attributed to the low-lying phonons arising from the low-frequency vibration of the Ir 5d states. The major contribution

of Ir $5d$ states near the Fermi level also gives rise to high SOC (SOC $\propto Z^4$). However, nodeless s-wave superconductivity and the presence of time-reversal symmetry (TRS) is quite surprising and suggests conventional superconductivity in spite of strong SOC and low-lying excitation mediating Cooper pairing. Moreover, the polycrystalline nature of IrGe and the existence of dirty limit superconductivity can suppress the anisotropy and nodes in the superconducting gap due to the large scattering. Therefore, further TF measurements on a high quality single crystal are required to exactly determine the role of the above mentioned mechanism on the superconducting gap structure. In order to obtain the penetration depth at $T = 0$ K, the following expression is used which is valid for $\kappa \geqslant 5$ and for an applied magnetic field much less than $H_{C2}(0)$:

$$5.814 \times \sigma_{FLL}(\mu s^{-1}) = \gamma_\mu \Phi_0 (1-h)[1+1.21(1-\sqrt{h})^3]\lambda^{-2},$$
(11)

where $h = H/H_{C2}(0)$ and Φ_0 is the magnetic flux quantum [41]. Using the values of $\sigma_{FLL}(0) = 4.1$ μs^{-1} and $H_{C2}(0) = 1.13$ T, we obtained $\lambda^{\mu SR}(0) = 1340$ (16) Å.

D. Electronic properties and Uemura plot

In order to confirm the dirty/clean limit superconductivity, the BCS coherence length, ξ_0, and mean free path, l_e, were determined. Based on the Drude model [31], the mean free path can be estimated using the expression $l_e = v_F \tau$ where τ is the scattering time and is given by $\tau^{-1} = ne^2\rho_0/m^*$. m^* is the effective mass of the quasiparticles, and can be evaluated using the following relation: $m^* = (\hbar k_F)^2 \gamma_n / \pi^2 n k_B^2$ where k_F is the Fermi wave vector. Considering a spherical Fermi surface and using the obtained value of $n = 1.27(2) \times 10^{28}$ m^{-3} from Hall measurement, $k_F = (3\pi^2 n)^{1/3}$ was estimated as 0.73(1) Å^{-1}. After incorporating the obtained values of k_F and n together with $\gamma_n = 1.73 \times 10^2$ J m^{-3} K^{-2}, we obtained $m^* = 4.6(4)m_e$. The Fermi velocity can be determined from the expression $v_F = \hbar k_F / m^* = 1.8(1) \times 10^5$ m/s. Using the values of n, m^*, v_F, and $\rho_0 = 5.57 \times 10^{-7}$ Ω m, l_e is estimated to be 41(6) Å. Within the BCS theory, coherence length (ξ_0) is defined as $0.18\hbar v_F / k_B T_C$, which yields $\xi_0 = 534(33)$ Å. The ratio of $\xi_0/l_e = 13(2)$ indicates the dirty limit superconductivity in IrGe. Using the values of $n = 1.27(2) \times 10^{28}$ m^{-3} and $m^* = 4.6(4)m_e$, the effective Fermi temperature of a three-dimensional system can be calculated by the following relation [42]: $k_B T_F = (3\hbar^3 \pi^2 n)^{2/3}/2m^*$, which came out to be 5088(469) K. The Fermi temperature is also calculated using the μSR and specific heat results via the expression $T_F = 730\sigma^{3/4}\gamma^{-1/4}$ where σ is in μs^{-1} and γ in mJ/cm^3 K^2 [43]. All the extracted values are tabulated in Table II. The low value of T_F from μSR results might be originated due to some percentage of error in penetration depth from muon results because of the nonaccountability of the Van Hove singularity smearing factor, arising from the increasing degree of disorderliness (one out of other possible reasons) [40].

Superconductors can be classified as conventional/unconventional based on the ratio of T_C/T_F provided by Uemura *et al.* [44–48]. Compounds belonging to different classes such as heavy fermions, Chevrel phases, high T_C, and Fe-based superconductors fall into the category of unconven-

TABLE II. Superconducting and normal state parameters of IrGe determined form various measurements.

Parameters	Unit	IrGe
T_C	K	4.74(3)
$H_{C1}(0)$	mT	13.3(2)
$H_{C2}(0)$	T	1.13(2)
$\Delta C_{el}/\gamma_n T_C$		2.7
θ_D	K	160(1)
λ_{e-ph}		0.78(2)
$\frac{\Delta^{SH}(0)}{k_B T_C}$		2.3(1)
$\frac{\Delta^\mu(0)}{k_B T_C}$		2.1(1)
ξ_{GL}	Å	170(1)
$\lambda_{GL}^{bulk,\mu SR}$	Å	1750(11),1340(16)
κ_{GL}		10(1)
n	$10^{28} m^{-3}$	1.27(2)
m^*	m_e	4.6(4)
l_e	Å	41(6)
ξ_0	Å	534(33)
$T_F^{bulk,\mu SR}$	K	5088(469),3272(109)

tional as their ratio lies in the $0.01 \leqslant T_C/T_F \leqslant 0.1$ range. The obtained value of $T_C/T_F = 0.0009$ for IrGe lies significantly outside the range of unconventional superconductors as is shown by a hollow red marker in Fig. 7. The result is surprising as IrGe falls in the strong-coupling regime which cannot be explained by the BCS theory, yet it is placed away from the band of unconventionality.

In summary, a detailed examination of the physical properties of IrGe is reported using various techniques which confirmed the bulk nature of superconductivity by exhibiting a T_C at 4.74(3) K. All the obtained parameters related to the superconducting and normal state are listed in Table II.
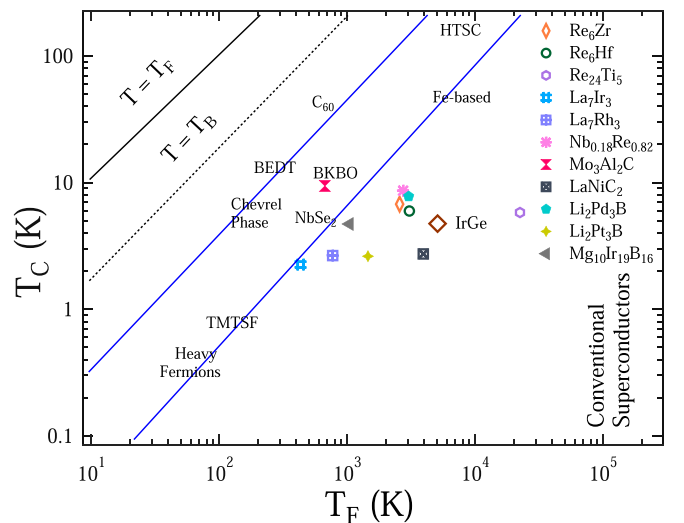

FIG. 7. Uemura plot representing transition temperature versus Fermi temperature for various superconductors belonging to different classes where the region between two solid blue lines represents the band of unconventionality. IrGe is represented by a hollow red marker.

Zero-field specific heat and TF-μSR studies reveal an isotropic nodeless superconductivity in strong-coupling regime. The results are in contrast to other low excitations mediated strongly coupled superconductors where anisotropic, multigap, and multiband type superconducting gap structure were observed. Zero-field μSR provide evidence of the absence of time-reversal symmetry breaking in IrGe. Therefore, from the microscopic measurements, the rattling mediated superconductivity in IrGe seems to be of conventional type. However, the strong-coupling nature originated from the rattling modes still seeks further examination through a detailed theoretical investigation of the Fermi surface and single crystal measurements.

[1] M. Grabowski, J. Phys. C: Solid State Phys. **20**, L735 (1987).

[2] Z. J. Yao, J. X. Li, and Z. D. Wang, New J. Phys. **11**, 025009 (2009).

[3] T. Takimoto and P. Thalmeier, J. Phys. Soc. Jpn. **78**, 103703 (2009).

[4] Y. Tada, N. Kawakami, and S. Fujimoto, J. Phys. Soc. Jpn. **77**, 054707 (2008).

[5] J. Chen and H. Q. Yuan, J. Phys.: Conf. Ser. **400**, 022010 (2012).

[6] M. Smidman, M. B. Salamon, H. Q. Yuan, and D. F. Agterberg, Rep. Prog. Phys. **80**, 036501 (2017).

[7] C. Kallin, Rep. Prog. Phys. **75**, 042501 (2012).

[8] E. F. Talantsev, K. Iida, T. Ohmura, T. Matsumoto, W. P. Crump, N. M. Strickland, S. C. Wimbush, and H. Ikuta, Sci. Rep. **9**, 14245 (2019).

[9] A. D. Hillier, J. Quintanilla, B. Mazidian, J. F. Annett, and R. Cywinski, Phys. Rev. Lett. **109**, 097001 (2012).

[10] F. Giubileo, D. Roditchev, W. Sacks, R. Lamy, and J. Klein, Europhys. Lett. **58**, 764 (2002).

[11] M. Furuyama, N. Kobayashi, and Y. Muto, Phys. Rev. B **40**, 4344 (1989).

[12] A. C. Gandhi and S. Y. Wu, Sci. Rep. **7**, 9442 (2017).

[13] L. R. Testardi, Rev. Mod. Phys. **47**, 637 (1975).

[14] S. D. Bader, G. S. Knapp, S. K. Sinha, P. Schweiss, and B. Renker, Phys. Rev. Lett. **37**, 344 (1976).

[15] T. Takayama, K. Kuwano, D. Hirai, Y. Katsura, A. Yamamoto, and H. Takagi, Phys. Rev. Lett. **108**, 237001 (2012).

[16] R. Lortz, Y. Wang, U. Tutsch, S. Abe, C. Meingast, P. Popovich, W. Knafo, N. Shitsevalova, Yu. B. Paderno, and A. Junod, Phys. Rev. B **73**, 024512 (2006).

[17] Z. Hiroi, S. Yonezawa, Y. Nagao, and J. Yamaura, Phys. Rev. B **76**, 014523 (2007).

[18] R. Khasanov, D. G. Eshchenko, D. Di Castro, A. Shengelaya, F. La Mattina, A. Maisuradze, C. Baines, H. Luetkens, J. Karpinski, S. M. Kazakov, and H. Keller, Phy. Rev. B **72**, 104504 (2005).

[19] A. Koda, W. Higemoto, K. Ohishi, S. R. Saha, R. Kadono, S. Yonezawa, Y. Muraoka, and Z. Hiroi, J. Phys. Soc. Jpn. **74**, 1678 (2005).

[20] R. Khasanov, A. Amato, P. K. Biswas, H. Luetkens, N. D. Zhigadlo, and B. Batlogg, Phys. Rev. B **90**, 140507(R) (2014).

[21] B. Wang, Y. Zhang, S. Xu, K. Ishigaki, K. Matsubayashi, J.-G. Cheng, H. Hosono, and Y. Uwatoko, Chin. Phys. B **28**, 107401 (2019).

[22] D. Hirai, M. N. Ali, and R. J. Cava, J. Phys. Soc. Jpn. **82**, 124701 (2013).

[23] H. M. Tütüncüa, H. Y. Uzunoka, E. Karacaa, S. Bağci, and G. P. Srivastava, Intermetallics **106**, 107 (2019).

[24] A. D. Hillier, J. S. Lord, K. Ishida, and C. Rogers, Philos. Trans. R. Soc. A **377**, 20180064 (2019)

[25] Z. Fisk and G. W. Webb, Phys. Rev. Lett. **36**, 1084 (1976).

[26] E. Helfand and N. R. Werthamer, Phys. Rev. **147**, 288 (1966).

[27] N. R. Werthamer, E. Helfand, and P. C. Hohenberg, Phys. Rev. **147**, 295 (1966).

[28] A. B. Karki, Y. M. Xiong, I. Vekhter, D. Browne, P. W. Adams, D. P. Young, K. R. Thomas, Julia Y. Chan, H. Kim, and R. Prozorov, Phys. Rev. B **82**, 064512 (2010).

[29] J. K. Bao, J. Y. Liu, C. W. Ma, Z. H. Meng, Z. T. Tang, Y. L. Sun, H. F. Zhai, H. Jiang, H. Bai, C. M. Feng, Z. A. Xu, and G. H. Cao, Phys. Rev. X **5**, 011013 (2015).

[30] K. Maki, Phys. Rev. **148**, 362 (1966).

[31] M. Tinkham, *Introduction to Superconductivity*, 2nd ed. (McGraw-Hill, New York, 1996).

[32] T. Klimczuk, F. Ronning, V. Sidorov, R. J. Cava, and J. D. Thompson, Phys. Rev. Lett. **99**, 257004 (2007).

[33] D. Singh, J. A. T. Barker, A. Thamizhavel, D. McK. Paul, A. D. Hillier, and R. P. Singh, Phys. Rev. B **96**, 180501(R) (2017).

[34] W. L. McMillan, Phys. Rev. **167**, 331 (1968).

[35] S. K. Ghosh, M. Smidman, T. Shang, J. F. Annett, Adrian D. Hillier, J. Quintanilla, and H. Yuan, J. Phys.: Condens. Matter **33**, 033001 (2021).

[36] R. S. Hayano, Y. J. Uemura, J. Imazato, N. Nishida, T. Yamazaki, and R. Kubo, Phys. Rev. B **20**, 850 (1979).

[37] P. K. Biswas, A. D. Hillier, M. R. Lees, and D. McK. Paul, Phys. Rev. B **85**, 134505 (2012).

[38] P. K. Biswas, S. K. Ghosh, J. Z. Zhao, D. A. Mayoh, N. D. Zhigadlo, Xiaofeng Xu, C. Baines, A. D. Hillier, G. Balakrishnan, and M. R. Lees, Nat. Commun. **12**, 2504 (2021).

[39] M. Weber, A. Amato, F. N. Gygax, A. Schenck, H. Maletta, V. N. Duginov, V. G. Grebinnik, A. B. Lazarev, V. G. Olshevsky, V. Y. Pomjakushin, S. N. Shilov, V. A. Zhukov, B. F. Kirillov, A. V. Pirogov, A. N. Ponomarev, and V. G. Storchak, S. Kapusta, and J. Bock, Phys. Rev. B **48**, 13022 (1993).

[40] A. Maisuradze, R. Khasanov, A. Shengelaya, and H. Keller, J. Phys.: Condens. Matter **21**, 075701 (2009).

[41] E. H. Brandt, Phys. Rev. B **68**, 054506 (2003).

[42] A. D. Hillier and R. Cywinski, Appl. Magn. Reson. **13**, 95 (1997).

[43] V. H. Tran, A. D. Hillier, D. T. Adroja, and D. Kaczorowski, J. Phys.: Condens. Matter **22**, 505701 (2010).

[44] Y. J. Uemura, G. M. Luke, B. J. Sternlieb, J. H. Brewer, J. F. Carolan, W. N. Hardy, R. Kadono, J. R. Kempton, R. F. Kiefl, S. R. Kreitzman, P. Mulhern, T. M. Riseman, D. L. Williams, B. X. Yang, S. Uchida, H. Takagi, J. Gopalakrishnan, A. W. Sleight, M. A. Subramanian, C. L. Chien *et al.*, Phys. Rev. Lett. **62**, 2317 (1989).

[45] K. Hashimoto, K. Cho, T. Shibauchi, S. Kasahara, Y. Mizukami, R. Katsumata, Y. Tsuruhara, T. Terashima, H. Ikeda, M. A. Tanatar, H. Kitano, N. Salovich, R. W. Giannetta, P. Walmsley, A. Carrington, R. Prozorov, and Y. Matsuda, Science **336**, 1554 (2012).

[46] R. Khasanov, H. Luetkens, A. Amato, H. H. Klauss, Z. A. Ren, J. Yang, W. Lu, and Z. X. Zhao, Phys. Rev. B **78**, 092506 (2008).

[47] Y. J. Uemura, L. P. Le, G. M. Luke, B. J. Sternlieb, W. D. Wu, J. H. Brewer, T. M. Riseman, C. L. Seaman, M. B. Maple, M. Ishikawa, D. G. Hinks, J. D. Jorgensen, G. Saito, and H. Yamochi, Phys. Rev. Lett. **66**, 2665 (1991).

[48] Y. J. Uemura, V. J. Emery, A. R. Moodenbaugh, M. Suenaga, D. C. Johnston, A. J. Jacobson, J. T. Lewandowski, J. H. Brewer, R. F. Kiefl, S. R. Kreitzman, G. M. Luke, T. Riseman, C. E. Stronach, W. J. Kossler, J. R. Kempton, X. H. Yu, D. Opie, and H. E. Schone, Phys. Rev. B **38**, 909 (1988).

[49] https://doi.org/10.5286/ISIS.E.100680288.